21st Australasian Fluid Mechanics Conference
Adelaide, Australia
10-13 December 2018

Downstream Recovery of Turbulence Kinetic Energy in the Wake of a Turbulent Boundary Layer Wing-Body Junction Flow

S. Zimmerman[1], J. Philip[1], N. Marino[2] and J. Klewicki[1,2]

[1]Department of Mechanical Engineering
University of Melbourne, Parkville, Victoria 3010, Australia

[2]Department of Mechanical Engineering
University of New Hampshire, Durham, New Hampshire 03824, USA

Abstract

A multi-sensor hotwire probe capable of simultaneously measuring all three components of the velocity vector [Zimmerman *et al.* 2017] has been deployed in the wake of a turbulent boundary layer wing-body junction flow. The wing shape—a 3:2 semi-elliptic nose joined to a NACA 0020 airfoil tail—matches that used in a number of existing studies of wing-body junction wake flow (e.g. see the review of Simpson [2001]). Data have been collected in four spanwise/wall-normal measurement planes ranging from 1 to 33 chord lengths behind the trailing edge of the junction. The measurement planes span a domain over which the unperturbed boundary layer would develop from friction Reynolds number $Re_\tau \approx 8000-11000$. The downstream extent (per chord length) of the present data is the furthest of any experimental effort to date. Despite having a recovery length many times longer than the typical streamwise wavelength of boundary layer 'superstructure' motions [Hutchins and Marusic 2007], the turbulence kinetic energy (TKE) profiles at the furthest downstream station still exhibit spanwise inhomogeneity. Data from the measurement planes closer to the junction offer insight into the momentum and turbulence transporting effects of the trailing 'horseshoe' vortex, as well as how these effects propagate downstream.

Introduction

Many flows of practical significance involve the interaction between an otherwise canonical zero pressure gradient boundary layer and a surface-mounted obstacle. Surface mounted obstacles of this kind result in highly three-dimensional mean flow fields in the vicinity of the body and its near-wake. Cases where the obstacle is streamlined, in particular, have been the subject of intensive research (e.g. see the review of [5]). Most streamlined-wing junction flow studies conducted thus far have focused on the unsteady behaviour of the "horseshoe" or "necklace" vortex that forms from the roll-up of spanwise vorticity from the mean boundary layer upstream of the leading edge. This spanwise vorticity is stretched and tilted into the streamwise direction by the mean velocity gradients around the wing. The resulting streamwise vorticity tends to draw high momentum fluid toward the bounding wall near the centerline, and eject low momentum fluid away from the bounding wall further outboard. While this phenomenon is well-documented, relatively few studies have examined the evolution of the junction-induced disturbance with downstream distance. [1] presented measurements of streamwise velocity as far as 10.56 chord-lengths behind the trailing edge of a streamlined Rood wing (3:2 elliptical leading edge joined to a NACA 0020 tail). In that study, however, the zero pressure gradient in-flow was transitioned to an adverse pressure gradient 6 chord-lengths behind the trailing edge to mimic the flow over the tapering portion of a submarine downstream of the conning tower. The present study examines the relaxation of the flow in the far wake of the junction back toward a statistically two-dimensional zero-pressure-gradient boundary layer.

Apart from elucidating the underlying physics, measurements of the TKE in complex flows hold the capacity to aide in the development of computational models (especially RANS) of complex geometries. Although many RANS models may produce satisfactory outputs in one particular class of flow geometries, they often struggle to generalise to others. For example, the well-known k-ε model with input coefficients suitable for a turbulent boundary layer will over-predict the spreading rate of an axisymmetric jet by about 40% [4]. New models may be trained on high-resolution experimental data at high Reynolds numbers (such as those presented here) across a wide range of flow geometries to handle cases that would otherwise result in model failure.

Experiments

The present data were collected at the Flow Physics Facility (FPF) at the University of New Hampshire. The FPF, characterised in detail by [6], is an open-circuit zero-pressure-gradient boundary layer facility with a flow development length of 72 meters. The scale of the FPF allows achievement of friction Reynolds numbers ($Re_\tau \equiv \delta_{99}u_\tau/\nu$) in excess of 10^4 without rendering the smallest energetic scales unresolvable by conventional measurement techniques. Streamwise/wall-normal velocity and spanwise vorticity measurements collected at the FPF under ZPG conditions are presented in [3], and three-component velocity and vorticity measurements are presented in [7].

The streamlined obstacle, a "Rood wing", was placed in the FPF at a 0° angle-of-attack with its leading edge 30.6m downstream of the turbulence trip. A schematic of the in-flow boundary layer and the four measurement planes is shown in figure 1.

Three component velocity data were acquired in y-z planes at each of the four streamwise (x) measurement stations by means of an 8-sensor hot-wire anemometry probe first described by [7]. Each measurement plane is comprised of a grid of 8 linearly-spaced spanwise positions and 10 logarithmically-spaced wall-normal positions. The measurement probe effectively consists of four independent $\times$-wire pairs, arranged such that all three velocity and vorticity components may be estimated simultaneously about the centroid of the measurement volume. The present experiments are unique in the downstream fetch of the observations, their quantification of the turbulence kinetic energy, the Re_τ of the in-flow boundary layer, and the high resolution of the measurements.

Results

Contours of mean streamwise velocity $\overline{U}$ normalized by the free-stream velocity U_o are shown for each of the four stream-

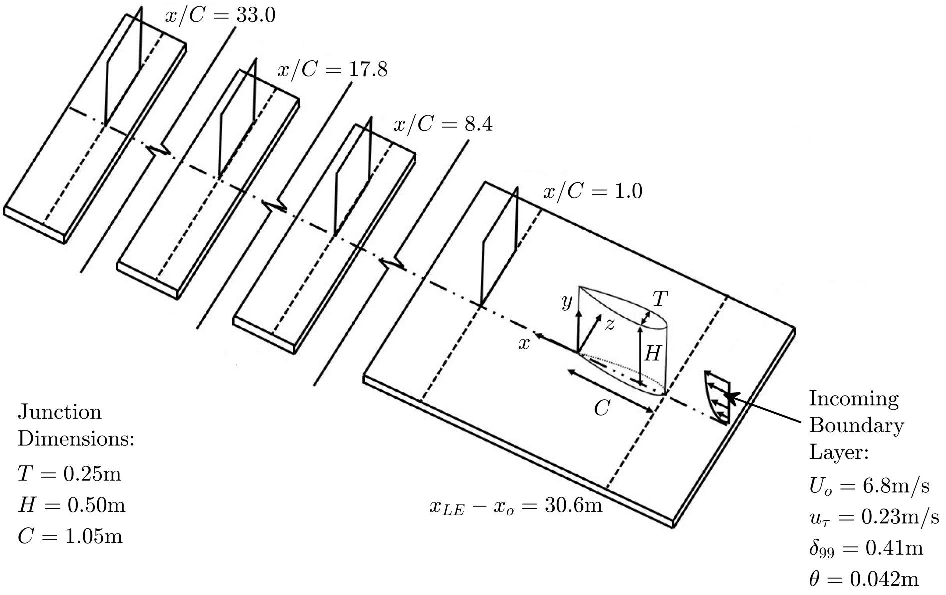

Figure 1: Schematic of the present flow geometry and y-z measurement plane locations. Note x_o refers to the location of the turbulence trip point in the FPF, and x_{LE} refers to the streamwise position of the leading edge of the Rood wing.

wise measurement stations in figure 2. Also shown in figure 2 are the differences between $\overline{U}/U_o$ for the junction-flow wake and the unperturbed ZPG boundary layer. The footprint of the secondary flow on $\overline{U}$ is clearly visible at $x/C = 1$, as shown in figures 2(a) and 2(b). The curvature of the U/U_o contours below $y/T \approx 1$ and inboard of $z/T \approx 2$ at this location reflects the mean momentum transport associated with the horseshoe vortex. The negative-oriented mean streamwise vorticity Ω_x tends to lift low-momentum boundary layer fluid away from the wall in a region bounded approximately by $0.5 \lesssim z/T \lesssim 1.7$, and draws high-momentum fluid toward the wall inboard of $z/T \approx 0.5$. The primary horseshoe vortex may also induce additional streamwise vorticity further outboard, as evidenced by the contours in figures 2(a) and (b) in the region bounded by $z/T \gtrsim 2.5$ and $y/T \lesssim 1$. The wake of the Rood wing above its junction with the wall is also visible in the $x/C = 1$ plane in the form of a momentum deficit in the region bounded by $1 \lesssim y/T \lesssim 3$ and $z/T \lesssim 1$. That the momentum deficit at $x/C = 1$ extends above $y/T = 2$ (or $y/H = 1$) suggests that high momentum regions further downstream are not caused by the 'downwash' of free stream flow over the obstruction, but rather are related to the secondary flow. Thus, it is unlikely that the downstream flow structure would be substantially affected by an increase in the height of the obstruction.

Several changes are observed in the organization of the flow behind the obstruction with downstream distance. By $x/C = 8.4$, the footprint of the horseshoe vortex has spread in both the y and z directions, and the wake of the Rood wing away from the junction is considerably weaker. Further downstream at the $x/C = 17.8$ and $x/C = 33$ planes, a high-momentum 'core' persists and maintains spanwise inhomogeneity, but weakens in magnitude and appears to spread appreciably only in the y direction. This is consistent with the observations of [1], that the horseshoe vortex 'legs' have an approximately constant width beyond $x/C = 5$, and that further spreading is caused primarily by boundary layer growth.

The spanwise spreading of the overall disturbance is apparent in the dependence of the momentum deficit on streamwise and spanwise position. This dependence is represented here through the quantity Θ_T, defined in equations (1) and (2) and plotted in figure 3.

$$\theta_T = \int_0^T \frac{\overline{U}}{U_o}\left(1 - \frac{\overline{U}}{U_o}\right) dy \tag{1}$$

$$\Theta_T = \frac{\theta_T - \theta_{T,ZPG}}{\theta_{T,ZPG}} \tag{2}$$

This quantity represents the proportional difference between the momentum deficit of the junction wake and that of the ZPG boundary layer for the region below $y/T = 1$, where the secondary flow is most prominent in the junction wake and the entirety of the inner-and logarithmic-layers are contained for all of the comparison ZPG boundary layer cases. The peak momentum deficit in the region of interest is found at $z/T \approx 1.3$ for the $x/C = 1$ plane. The peak is less distinct (or non-existent) at the next three measurement locations, though the region of decreased momentum deficit thickness extends to slightly larger values of z/T for each successive location.

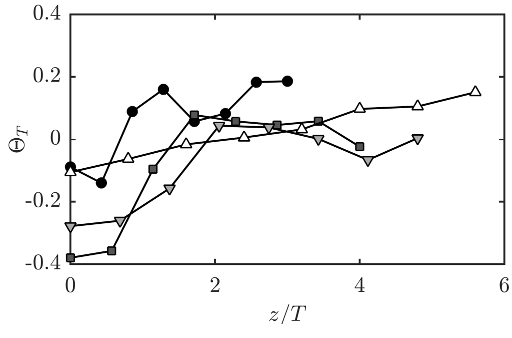

Figure 3: Proportional difference in momentum deficit thickness between junction flow wake and ZPG below $y/T = 1$ for (symbols darkest to lightest) $x/C = 1$, $x/C = 8.4$, $x/C = 17.8$, and $x/C = 33.0$

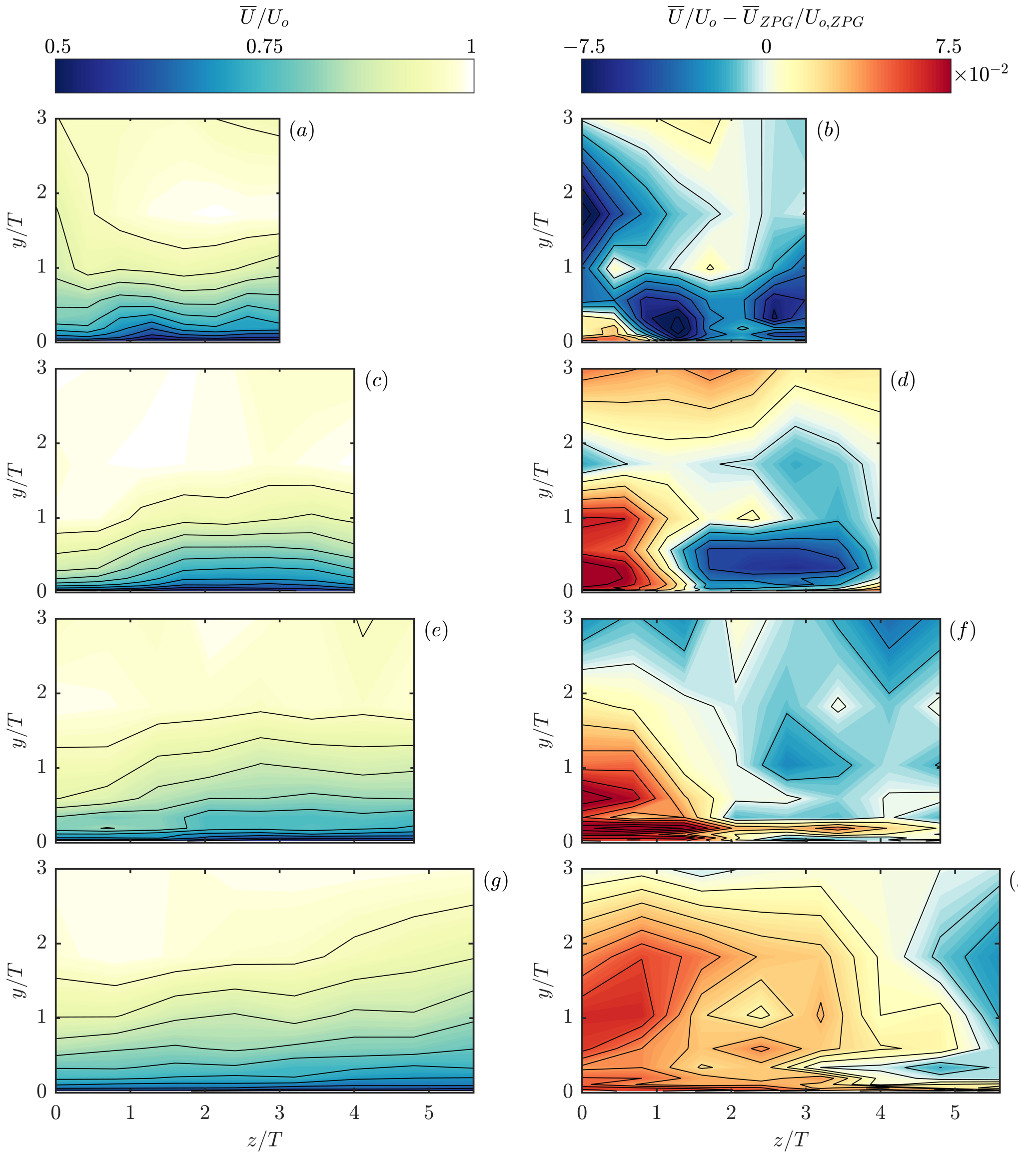

Figure 2: Mean streamwise velocity contours ($(a),(c),(e),(g)$) and their difference from unperturbed ZPG case ($(b),(d),(f),(h)$) for y-z measurement planes at $(a),(b)$: $x/C = 1.0$, $(c),(d)$: $x/C = 8.4$, $(e),(f)$: $x/C = 17.8$ and $(g),(h)$: $x/C = 33.0$.

Figure 4 shows the mean turbulence kinetic energy $\overline{k}$ in the junction flow wake as well as the difference in $\overline{k}$ between the junction flow wake and the unperturbed ZPG boundary layer for the four measurement planes. Low momentum regions (relative to the ZPG case) identified above each exhibit higher turbulence kinetic energy than the comparable ZPG case, while those having higher mean momentum each exhibit lower turbulence kinetic energy. In the regions affected by the secondary flow, this reflects the mixing associated with the horseshoe vortex. High momentum boundary layer fluid drawn toward the wall transports with it lower turbulence kinetic energy, while low momentum fluid ejected away from the wall caries energetic motions associated with the near-wall flow. In the region bounded by $z/T \lesssim 1$ and $y/T \gtrsim 1$ at $x/C = 1$, the high turbulence kinetic energy relative to the ZPG case is reflective of the wake of the wing and not the secondary flow. As with the mean momentum, the 'core' of low $\overline{k}$ initially associated with the secondary flow spreads primarily in the y-direction with downstream distance as the boundary layer continues to grow.

Conclusions

Mean velocity and turbulence kinetic energy were acquired in the wake of a turbulent wing-body junction flow via multi-sensor hot-wire anemometry. These data capture the near-wake characteristics of the horseshoe vortex, as well as its downstream evolution and associated relaxation of the flow field toward spanwise homogeneity. The far wake behind the junction is characterised by higher momentum close to the centerline and lower momentum further outboard. This is the opposite of a typical bluff-body wake, indicating that the transport of momentum associated with the secondary flow dominates over loss of momentum associated with the net drag around the wing within the boundary layer. The momentum deficit behind the wing extends above $y/H = 1$, indicating that the high momentum 'core' region does not owe its existence to the low δ/H ratio of the present experiment. The high momentum core can be seen through the momentum deficit thickness to spread with downstream distance. The momentum deficit thickness at the furthest downstream position ($x/C = 33.0$) varies approximately linearly with z.

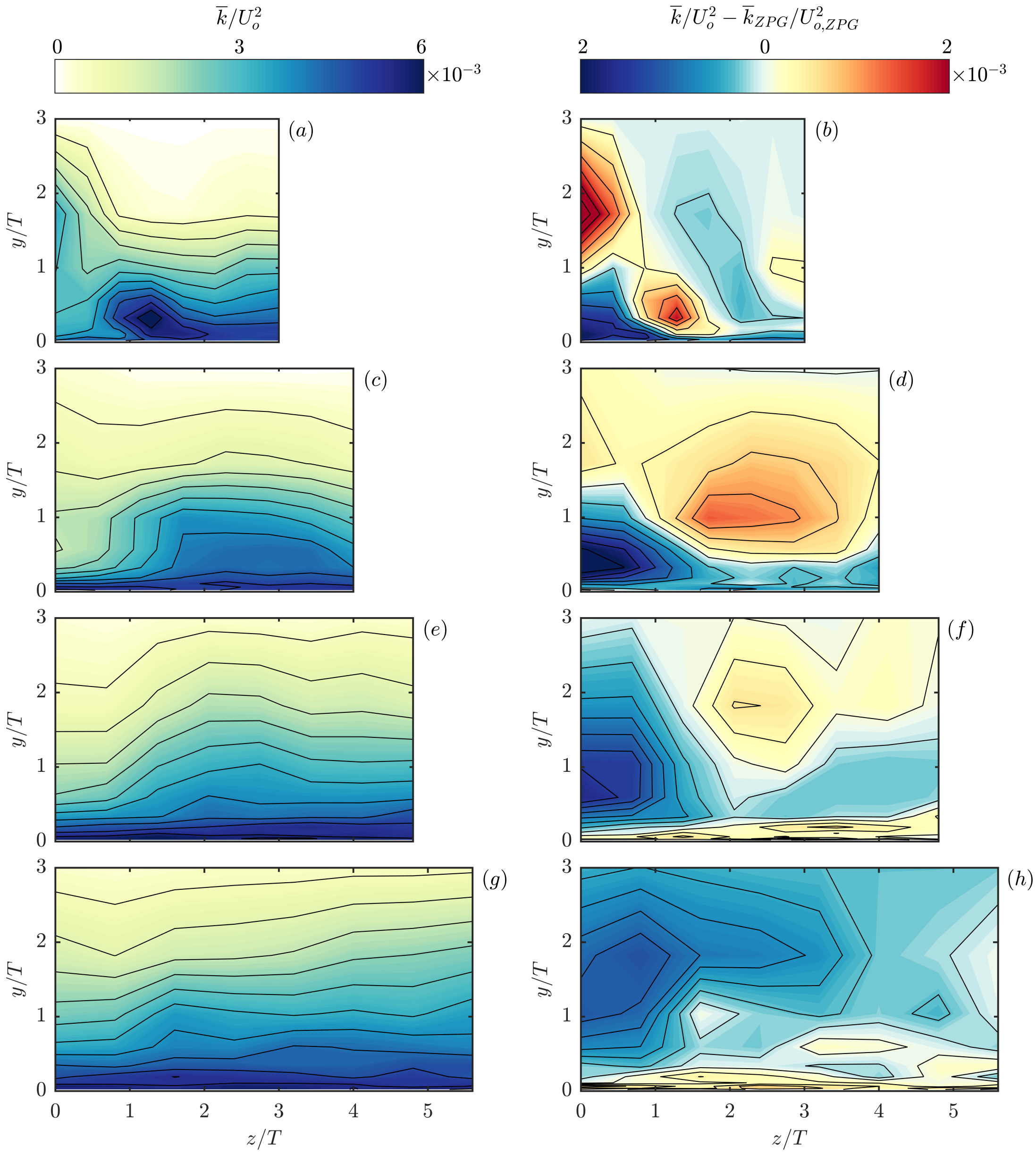

Figure 4: Mean turbulence kinetic energy contours $((a),(c),(e),(g))$ and their difference from unperturbed ZPG case $((b),(d),(f),(h))$ for y-z measurement planes at $(a),(b)$: $x/C = 1.0$, $(c),(d)$: $x/C = 8.4$, $(e),(f)$: $x/C = 17.8$ and $(g),(h)$: $x/C = 33.0$.

Acknowledgements

This work was supported by the Australian Research Council and the Office of Naval Research under award number N00014-17-1-2307.

References

[1] Fleming, J. L., Simpson, R. L., Cowling, J. E., and Devenport, W. J., An experimental study of a turbulent wing-body junction and wake flow. *Exp. Fluids*, **14**(5), 1993, 366–378.

[2] Hutchins, N., and Marusic, I., Evidence of very long meandering features in the logarithmic region of turbulent boundary layers. *J. Fluid Mech.*, **579**, 2007, 1–28.

[3] Morrill-Winter, C., Philip, J., Klewicki, J., An invariant representation of mean inertia: theoretical basis for a log law in turbulent boundary layers. *J. Fluid Mech.*, **813**, 2017, 594–617.

[4] Pope, S. B., An explanation of the turbulent round-jet/plane-jet anomaly. *AIAA J.* **16**(3) 1978, 279–281.

[5] Simpson, R. L., Junction flows. *Ann. Rev. Fluid Mech.*, **33**(1), 2001, 415–443.

[6] Vincenti, P., Klewicki, J., Morrill-Winter, C., White. C. M., and Wosnik, M., Streamwise velocity statistics in turbulent boundary layers that spatially develop to high Reynolds number. *Exp. Fluids*, **54**(12), 2013, 1629.

[7] Zimmerman S., Morrill-Winter C., and Klewicki J., Design and implementation of a hot-wire probe for simultaneous velocity and vorticity vector measurements in boundary layers. *Exp. Fluids*, **58**(10), 2017, 148.